IEEE Access
Multidisciplinary | Rapid Review | Open Access Journal

SPECIAL SECTION ON CYBER-PHYSICAL-SOCIAL COMPUTING AND NETWORKING

Received September 11, 2017, accepted November 6, 2017, date of publication November 23, 2017,
date of current version February 28, 2018.

Digital Object Identifier 10.1109/ACCESS.2017.2777185

Pseudo-Dynamic Network Modeling for PMU-Based State Estimation of Hybrid AC/DC Grids

WEI LI[1], (Student Member, IEEE), LUIGI VANFRETTI[2], (Senior Member, IEEE), AND JOE H. CHOW[2], (Life Fellow, IEEE)

[1]Department of Electric Power and Energy Systems, KTH Royal Institute of Technology, SE-100 44 Stockholm, Sweden
[2]Department of Electrical, Computer, and Systems Engineering, Rensselaer Polytechnic Institute, Troy, NY 12180 USA

Corresponding author: Wei Li (wei3@kth.se)

The work of W. Li was supported by the *SweGRIDS* Project. The work of L. Vanfretti and J. H. Chow was supported in part by the Engineering Research Center Program of the National Science Foundation and the Department of Energy under Award EEC-1041877 and in part by the CURENT Industry Partnership Program.

ABSTRACT This paper presents a PMU-based state estimation (SE) algorithm that uses a pseudo-dynamic network modeling approach. The pseudo-dynamic network model combines different equations with static network equations. Then it applies the weighted least squares algorithm to solve an over-determined least squares estimation problem. The proposed method can improve SE accuracy during both steady state and transient conditions without increasing the computational burden. In addition, the proposed modeling approach is applied to networks containing both a STATCOM and a voltage source converter-HVdc to demonstrate how to develop and apply a pseudo-dynamic SE model. Case studies aim to illustrate and verify the performance of the proposed method under steady state and transient conditions.

INDEX TERMS Pseudo-dynamic, PMU, state estimation, STATCOM, VSC-HVDC.

I. INTRODUCTION

Pmu-based state estimation (SE) is gradually becoming a practical and effective approach for power system monitoring and control [1]–[3]. Compared to the telemetry data used in conventional SCADA systems, PMUs provide measurements with a global time stamp and in a much higher reporting rate, which allows operators to enhance operational security and to perform post-contingency analyses [4]. In addition to the high resolution measurement data, PMUs directly measure the system states that are to be estimated, thus allowing to develop a state estimation network model with relatively low nonlinearity for the estimation algorithm to solve as compared with conventional SE approaches [4].

A. MOTIVATIONS

As renewable energy integration brings intermittent fluctuations into power systems, SE algorithms will face the need to capture system dynamics in a faster and more flexible way, which can be difficult for the conventional SEs. On the other hand, most of the so-called dynamic SEs, or forecasting-aided SEs, are computationally demanding, which introduces delays in the estimation calculation cycle [5]. When the calculation cycle is longer than the PMU data rate, the estimated results become less valuable for on-line applications, especially those with real-time requirements.

Therefore, this work proposes a pseudo-dynamic modeling approach that can improve the SE accuracy during transients without significantly increasing the SE's computational burden.

At the same time, this work aims to address how the power electronics-based devices (e.g., flexible AC transmission system (FACTS) and voltage source converter (VSC)-based HVDC links) can be included in PMU-based SEs. As their installations continue to increase worldwide, these technologies will play an important role in improving the system control ability and flexibility with the increased integration of renewable energy. Therefore, their real-time performance during transients needs to be monitored in order to make full use of these devices in on-line operations. To this end, this work develops suitable pseudo-dynamic models that can represent power electronics-based devices for both steady state and transient conditions.

B. RELATED WORKS

Work on tracking [6] and dynamic [7] SEs started as early as in the 1970s. In [6] the most recent estimated state set is used as a one-step prediction, which is not always valid particularly when the system is under transient operating conditions. Although [7] firstly introduces Kalman filter from aerospace applications to power system SE, adopting

oversimplified models to describe state's time evolution results in a relatively limited estimation capability. Since 1990s, efforts on including a predictive database are taken to enhance the SE process via developing appropriate system models or/and implementing probability analyses. Interested readers are referred to [8] that provides a comprehensive survey on this topic. To the authors' knowledge, this is the first article that proposes to combine a pseudo-dynamic model with a PMU-based static SE algorithm, i.e., weighted least squares (WLS).

Previous work on FACTS modeling for SEs has been conducted in the past decade. References [10]–[12] present FACTS models for the conventional static SEs using SCADA data. References [13]–[16] propose to use PMU data to conduct SEs for the networks containing FACTS devices. All the above work has focused on the static FACTS models for the static SEs, while this article proposes a pseudo-dynamic model for the STATCOM, as an example of FACTS devices.

HVDC modeling for SEs dates back to 1980's, when [17] first includes a classic HVDC link model into an AC system SE. Reference [18] presents a relatively simplified AC/DC converter model and extends it into a multi-terminal DC (MTDC) model for SEs. Reference [19] focuses on modeling classic HVDC links with only PMU measurements. With the rapid development and expansion of VSC-based devices, their SE models have also been studied. References [20] and [21] introduce a basic VSC model and a generic VSC-based MTDC model for SEs, respectively. Reference [22] combines SCADA data with PMU data for hybrid SEs of VSC-HVDC links. Reference [23] presents a more detailed VSC-HVDC link model for a PMU-only SE. This article proposes a pseudo-dynamic model for VSC-HVDC links in order to represent the dynamic behavior of VSC-based devices.

C. CONTRIBUTIONS

This article proposes a pseudo-dynamic modeling approach for PMU-based SEs, that offers the following contributions:

- High accuracy: It establishes difference equations from the dynamic model of certain components from both AC and DC grids, and then combines them with the static network equations. This process is named: *pseudo-dynamic network modeling*.
- Compatible modeling and implementation: The pseudo-dynamic network model maintains the basic structure of the static model, which greatly reduces the workload of re-composing network models when updating existing algorithms.
- Fast computation: the algorithm used to solve the static SE problem (WLS) is directly applied to the pseudo-dynamic SE, which ensures that the computational speed will be minimally affected.
- Explicit representation of control modes: For devices with time-varying control references, the pseudo-dynamic SE is capable of taking their control modes into account, which would be challenging for static-only SEs.

In addition, two power electronics-based devices are used to illustrate the proposed approach—static synchronous compensator (STATCOM), as an example of a FACTS device, and VSC-HVDC link.

This article is organized as follows. Section II presents the PMU-based SE algorithm and the pseudo-dynamic network modeling. The static and pseudo-dynamic network models for the STATCOM and the VSC-HVDC link are introduced in Section III and Section IV, respectively. Simulation results in Section V perform a comparison between the proposed pseudo-dynamic SE to the basic static SE. And Section VI compares their computation performance. Finally, some conclusions are drawn in Section VII.

II. PMU-BASED STATE ESTIMATION ALGORITHM

This section presents the PMU-based SE algorithm that can be applied for both static SE and pseudo-dynamic SE. The only difference that exits is in the network models: the static SE network model only contains static equations; while the pseudo-dynamic SE network model combines difference equations that describe system dynamical properties with static network equations. The network model is combined with a measurement model and the WLS is applied to solve the over-determined estimation problem.

A. WLS FORMULATION AND MEASUREMENT MODEL

The SE can be formulated as a nonlinear WLS problem with the objective of minimizing the discrepancy between the measured and the estimated values of each phasor quantity. In this work, the WLS problem is formulated as

$$\min_{\mathbf{x}} \sum_{i=1}^{n+m} w_i e_i^2, \tag{1}$$

where

$$\mathbf{e} = \begin{bmatrix} \mathbf{h}(\mathbf{x}) \\ \varepsilon \end{bmatrix}. \tag{2}$$

Here $\mathbf{e} \in \mathbb{R}^{n+m}$ is the error vector and e_i is the ith row; and w_i is the ith diagonal element of the weight matrix. m and n denote the number of measured quantities and network equations, respectively.

The error vector $\mathbf{e}$ contains two parts: 1) network model equations $\mathbf{h}(\mathbf{x}) \in \mathbb{R}^n$; 2) errors between the measurements and their corresponding states $\varepsilon \in \mathbb{R}^m$. Ideally, network equations would assume a perfect model, i.e., $\mathbf{h}(\mathbf{x}) = \mathbf{0}$, which is not the case in practice. Hence, this work considers the case when the network equations may contain modeling errors, and thus, weights based on the confidence in the model's accuracy are assigned to them. For the second part, as PMUs provide telemetry of the system states directly, the errors are for the quantities such as bus voltage magnitude $|\mathbf{V}|$ and angle θ, line current magnitude $|\mathbf{I}|$ and angle δ, and even other user-defined states, depending on what the PMUs are measuring.

The advantage of using Eq. (2) lies in the flexibility of granting different weights to different network model equations since they inherently have different accuracies due to disparate reliabilities of the model's parameters.

Due to space limitations, readers are referred to the nonlinear WLS solution in [1]–[3] and [19]. This article focuses on the enhancements to the network modeling, which will be presented in the following subsection.

B. NETWORK MODEL

When using PMU data, the network model $\mathbf{h}(\mathbf{x})$ can be formulated as linear functions. This process requires careful selection on states [4]. If the complex bus voltages and complex line currents are selected as states, $\mathbf{h}(\mathbf{x})$ is linear and the resulting estimation problem can be solved without iterations. However, in this article, bus voltage and line current phasors are defined in polar coordinates, that is, in the form of magnitudes and angles, leading to a nonlinear network model. This choice is relevant and important in order for the SE to inherently detect and correct phasor angle errors [3], [19], [24] due to time asynchronization [25]. As the magnitude and angle of a phasor quantity are largely independent variables in a PMU, the angle error will be a single variable in the polar coordinates instead of two error quantities in rectangular coordinates, which facilitates formulating angle errors in a straightforward fashion.

The network model for the static SE describes the system topology and properties under normal operating conditions, which can be considered to be in the quasi-stationary regime. However, when the system is under transient conditions, the static network model for certain components may no longer hold. If the models for such components are not replaced by the models that can represent their dynamic behaviors, the SE error would be significantly large. In other words, when the system enters a transient condition due to a perturbation, if the system cannot restore a steady state before the next PMU snapshot comes, the static network model will conflict with the PMU measurement, leading to an inaccurate SE solution.

Therefore, a new type network model, called here the *pseudo-dynamic network model*, is proposed. It leverages the existing body of the network model and includes the difference equations that describe the system dynamical properties. The following section explains how to formulate the pseudo-dynamic network model.

Typically, it is assumed that the power system as a continuous dynamical system can be described by employing differential equations. However, for PMU-based SE purposes, telemetry is streamed discretely over fixed and synchronous time intervals. In this sense, a power system can be treated as a discrete dynamical system, where difference equations are used to update the state variables in discrete time steps of the same size as the PMU data.

This discretization is similar to numerically solving differential equations, i.e. numerical integration, using Euler's method; where the states are updated when knowing the starting point and the slope at it, and the error can be made small if the step size is small enough and the interval of computation is finite. However, Euler's method is insufficiently robust, and thus the Euler's full-step modification, which belongs to a second-order Runge-Kutta method, is used next.

The difference equations used in this article are formulated as

$$\widehat{\mathbf{x}}_k \approx \mathbf{x}_{k-1} + \frac{T_s}{2}(\dot{\mathbf{x}}_{k-1} + \dot{\widehat{\mathbf{x}}}_k), \tag{3}$$

where T_s is the sample time (step size). $\dot{\mathbf{x}} = \mathbf{g}(\mathbf{x})$ can be either a linear or nonlinear function of $\mathbf{x}$, which is essentially the differential equation of the continuous dynamical system. The value of $\dot{\mathbf{x}}_{k-1}$ is calculated by substituting $\mathbf{x}_{k-1}$ into $\mathbf{g}(\mathbf{x})$, which is denoted by $\mathbf{g}(\mathbf{x})_{k-1}$.

Equation (3) implies that the present value is calculated by adding the average increment during the time interval to the previous value. In order to comply Eq. (3) with the generalized form of the network model equation $\mathbf{h}(\mathbf{x})$, it is rewritten as

$$\mathbf{h}(\mathbf{x_k}) : \widehat{\mathbf{x}}_k - \mathbf{x}_{k-1} - \frac{T_s}{2}\left(\mathbf{g}(\mathbf{x})_{k-1} + \mathbf{g}(\mathbf{x})_k\right). \tag{4}$$

The foregoing is the procedure of *pseudo-dynamic network modeling* and Eq. (4) is a *pseudo-dynamic network model*, which can be used to describe all different components with dynamical behavior. While the majority of the literature considers the use of Kalman Filters or other types of observers for a similar purpose, this work chooses a simpler approach, which only requires few PMU measurements close to a certain component and without the need of formulating a complex dynamic model. Two examples are presented in the following sections.

III. STATCOM NETWORK MODEL

This section introduces the static and pseudo-dynamic models of a STATCOM. The static model utilizes the static V-I characteristic when the STATCOM is under the linear operation range; while the pseudo-dynamic model includes the STATCOM's control process to better reflect its dynamic performance.

A. STATCOM STATIC MODEL

The STATCOM aims to control the voltage at the connected bus [26]. It has a linear voltage-current (V-I) relation when it is under steady state operation conditions. A typical terminal voltage versus output current characteristic is shown in Fig. 1. Hence, for static analysis purposes, a STATCOM can be modeled as an equivalent impedance, which is represented by the slope X_s. This characteristic can be determined by two points, $(0, V^{ref})$ and $(|I_0|, |V_0|)$. The latter point is any steady operating point in the V-I curve as long as the V^{ref} is not changed by the operator. Several PMU snapshots of the STATCOM voltage and current phasors allow to determine this linear V-I characteristic, as illustrated using real PMU data in Sec. V-A.

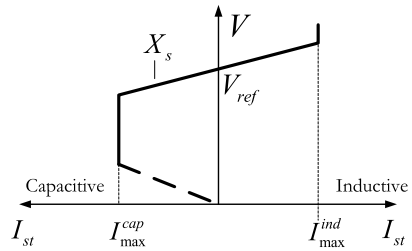

FIGURE 1. The voltage-current characteristic of STATCOMs.

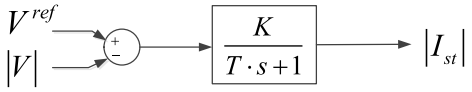

FIGURE 2. STATCOM control block diagram.

Using the V-I characteristic, its static network model can be formulated as [16]:

$$\mathbf{h(x)} : |V| - X_s|I_{st}| - V^{ref}, \tag{5}$$

where V is the bus voltage; V^{ref} is the preset voltage reference which the STATCOM aims to maintain; and I_{st} is the equivalent current phasor generated by the STATCOM.

Therefore, the states of an AC system with STATCOMs can be denoted as

$$\mathbf{x} = [|\mathbf{V}|, |\mathbf{I}|, \theta, \delta, |\mathbf{I_{st}}|]^T, \tag{6}$$

where $|\mathbf{V}|$, $|\mathbf{I}|$, θ and δ are AC system states. More details of AC network model can be found in [19].

B. STATCOM PSEUDO-DYNAMIC MODEL

This subsection introduces the pseudo-dynamic network model of a STATCOM. It is used as an example of how to develop a pseudo-dynamic network model for a controller.

The STATCOM's control process can be represented by the block diagram shown in Fig. 2. The output is the current magnitude $|I_{st}|$, which vary the current flow at the connected bus in order to change the reactive power flow and control the bus voltage. I_{st} is perpendicular to the bus voltage phasor, hence its angle can be computed from the voltage angle.

This controller model is given by

$$|\dot{I}_{st}| = \frac{K}{T}(V^{ref} - |V|) - \frac{1}{T}|I_{st}|. \tag{7}$$

Using the pseudo-dynamic network model described by Eq. (4), Eq. (7) can be written as:

$$\mathbf{h(x_k)} : \left(1 + \frac{T_s}{2T}\right)|\widehat{I}_{st,k}| + \frac{T_sK}{2T}|\widehat{V}_k| - \frac{T_sK}{T}V^{ref} - \left(1 - \frac{T_s}{2T}\right)|I_{st,k-1}| + \frac{T_sK}{2T}|V_{k-1}|. \tag{8}$$

Equation (8) embodies the dynamic relation between $|\widehat{V}|$ and $|\widehat{I}_{st}|$, and replaces the static relation in Eq. (5). This pseudo-dynamic network model of the STATCOM is validated using the real PMU data in Sec. V-A, and simulation studies in Sec. V-B.

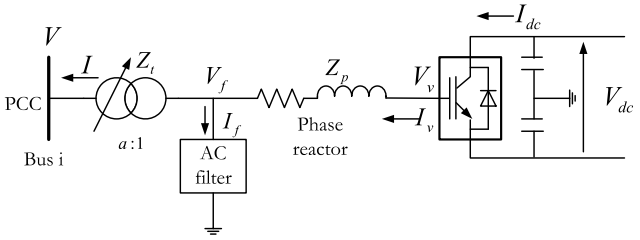

FIGURE 3. VSC substation structure.

The states of the new model are the same as those of the static model (Eq. (6)). The corresponding Jacobian matrix elements must be updated using

$$H(x_k) : \frac{\partial h(x_k)}{\partial |\widehat{I}_{st,k}|} = 1 + \frac{T_s}{2T}, \quad \frac{\partial h(x_k)}{\partial |\widehat{V}_k|} = \frac{T_sK}{2T}. \tag{9}$$

IV. VSC-HVDC NETWORK MODEL

This section presents a VSC-HVDC substation's static model, its pseudo-dynamic model, and a VSC-HVDC link's pseudo-dynamic model. The substation's static model uses the converter's voltage to represent its voltage reference. The reason why the voltage reference is not used as a state is because it is internally generated by the control system, and thus it cannot be considered in the static model. On the other hand, the pseudo-dynamic model includes the process of calculating this voltage reference, leading to a much more accurate model. Then the substation's pseudo-dynamic model is extended to a point-to-point VSC-HVDC link model by including a DC link model.

A. VSC SUBSTATION STATIC MODEL

Figure 3 shows a VSC substation structure: V, I are the voltage and current phasors at Bus i, which is also the point of common connection (PCC); V_f is the voltage phasor at the AC filter and I_f is the current phasor flowing into it; V_v and I_v are the voltage and current phasors at the AC side of the converter; Z_t and Z_p are the impedances of the transformer and phase reactor, respectively.

As indicated in Fig. 3, Bus i connects to the VSC substation through an AC line, which can be represented by the AC branch model to build up the relation between V, I, V_f, I_f and V_v, I_v. Hence, the static network model is formulated as [23]:

$$\mathbf{h(x)} : \begin{cases} V_v - V_f - I_vZ_p, \\ V_f - \dfrac{1}{a}V - aIZ_t, \\ I_v - I_f - aI. \end{cases} \tag{10}$$

Furthermore, in order to find the relation between converter's voltage and current phasors with the DC voltage and current, the converter model needs to be included. For SE purposes, an average value model (AVM) is sufficient for a VSC, which avoids distinguishing different switching levels and modulation types, and instead it focuses on the fundamental frequency voltage and current components. Therefore,

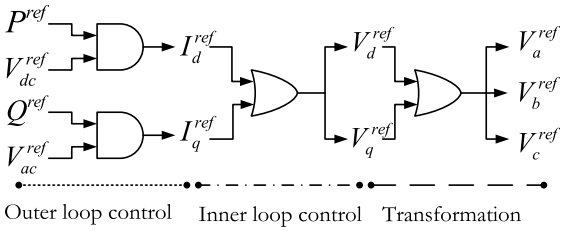

FIGURE 4. The vector-current control process for VSCs.

the converter model is formulated as [23] :

$$\mathbf{h(x)}: \begin{cases} M_v \dfrac{V_{dc}}{2} - |V_v|, \\ (K_{d2a})^2 \dfrac{V_{dc}}{2} I_{dc} - |V_v||I_v| \cos(\theta_v - \delta_v), \end{cases} \tag{11}$$

where M_v is the modulation index, which is defined here as the ratio of the root-mean-square (rms) value of the modulating wave, i.e., positive-sequence component of the AC voltage at the converter, to the peak value of the carrier wave, i.e., the pole-to-pole DC voltage; K_{d2a} is the coefficient that transfers DC quantities to the AC base when using per unit values; θ_v and δ_v are the converter voltage and current angles, respectively.

In summary, combining Eq. (10)-(11) gives a VSC substation model for static SE. The states of an AC system with VSC substations are given by

$$\mathbf{x} = [|\mathbf{V}|, |\mathbf{I}|, \theta, \delta, |\mathbf{V_f}|, \theta_\mathbf{f}, |\mathbf{I_f}|, \delta_\mathbf{f}, |\mathbf{V_v}|, \theta_\mathbf{v}, \mathbf{V_{dc}}, \mathbf{I_{dc}}]^T. \tag{12}$$

B. VSC SUBSTATION PSEUDO-DYNAMIC MODEL

In Eq. (11), the modulation index M_v defines the relation between V_{dc} and $|V_v|$. However, in reality $|V_v|$ varies with the system dynamics; while M_v is a fixed value that depends on the control mode. Therefore, in order to improve the accuracy of the model in Eq. (10)-(12) especially during transients, $|V_v|$ in Eq. (11) is replaced by $|v^{ref}|$, which is the converter bridges' voltage reference. This voltage reference is generated by the converter's control system.

The substation's pseudo-dynamic model intends to *represent* the control process of the converter. The most common control strategy for VSCs is vector-current control, which has a two-level control strategy, so-called the outer active-reactive power and voltage loop (here abbreviated to outer loop), and the inner current loop (here abbreviated to inner loop). As shown in Fig. 4, the outer loop transfers the VSC control references, i.e., P^{ref}, Q^{ref}, V_{dc}^{ref} and V_{ac}^{ref}, into the converter's current references, $\mathbf{i_{dq}^{ref}} = (i_d^{ref} \;\; i_q^{ref})^T$. In this strategy, three-phase fundamental currents and voltages are transformed into dq components in a synchronously rotating reference frame through Clark's and Park's transformations. Hence, all quantities become DC signals [28].

Depending on the converter's operation mode, reference i_d^{ref} can be determined by either active power P^{ref} or DC voltage V_{dc}^{ref}. Similarly, reference i_q^{ref} can be determined by either reactive power Q^{ref} or AC voltage V_{ac}^{ref} at the PCC. For each VSC substation, only one i_d^{ref} and only one i_q^{ref} can be utilized. An ordinary integral controller can be used for outer loop, which can be formulated using the pseudo-dynamic equations (Eq. 4) as:

$$\begin{aligned} \mathbf{h(x_k)}: \; & \widehat{i}_{d,k}^{ref} - i_{d,k-1}^{ref} - K_P \frac{T_s}{2}\left(\frac{P^{ref} - \widehat{P}_k}{|\widehat{V}_{f,k}|} + \frac{P^{ref} - \widehat{P}_{k-1}}{|V_{f,k-1}|}\right), \\ & \text{or } \widehat{i}_{d,k}^{ref} - i_{d,k-1}^{ref} - K_{Vdc} \frac{T_s}{2}\left(2V_{dc}^{ref} - \widehat{V}_{dc,k} - V_{dc,k-1}\right); \\ & \widehat{i}_{q,k}^{ref} - i_{q,k-1}^{ref} - K_Q \frac{T_s}{2}\left(\frac{Q^{ref} - \widehat{Q}_k}{|\widehat{V}_{f,k}|} + \frac{Q^{ref} - \widehat{Q}_{k-1}}{|V_{f,k-1}|}\right), \\ & \text{or } \widehat{i}_{q,k}^{ref} - i_{q,k-1}^{ref} - K_{Vac} \frac{T_s}{2}\left(2V_{ac}^{ref} - \widehat{V}_{ac,k} - V_{ac,k-1}\right); \end{aligned} \tag{13}$$

where $\widehat{P}_k = |\widehat{V}_k||\widehat{I}_k|cos(\widehat{\theta}_k - \widehat{\delta}_k)$, $\widehat{Q}_k = |\widehat{V}_k||\widehat{I}_k|sin(\widehat{\theta}_k - \widehat{\delta}_k)$.

Next, the outputs of the outer loop become the inner loop's input. The inner loop transfers the current references $\mathbf{i_{dq}^{ref}} = (i_d^{ref} \;\; i_q^{ref})^T$ into the voltage references of the converter bridges $\mathbf{v_{dq}^{ref}} = (v_d^{ref} \;\; v_q^{ref})^T$, which then are transformed into the three-phase voltage references. At last, a PWM algorithm is utilized to generate switching commands for each sub-module.

Based on the converter's structure shown in Fig. 3, the converter bridges' fundamental voltage equals to the voltage at PCC minus the voltage drop on the transformer and the phase reactor. By neglecting the resistances of the transformer and the phase reactor, an ordinary PI controller can be used for the inner loop, which is formulated as:

$$v^{ref} = V - (K_p + K_i \frac{1}{s})(i^{ref} - I_v) - j(X_t + X_p) i^{ref}, \tag{14}$$

where $\widehat{v}^{ref} = \widehat{v}_d^{ref} + j\widehat{v}_q^{ref}$ and $\widehat{i}^{ref} = \widehat{i}_d^{ref} + j\widehat{i}_q^{ref}$.

Equation (14) can be rewritten as:

$$\begin{aligned} \widehat{v}_k^{ref} = \widehat{V}_k - K_p\left(\widehat{i}_k^{ref} - \widehat{I}_{v,k}\right) - K_i \frac{1}{s}\left(\widehat{i}_k^{ref} - \widehat{I}_{v,k}\right) \\ - j(X_t + X_p)\widehat{i}_k^{ref}. \end{aligned} \tag{15}$$

In order to formulate Eq. (15) in the form of the pseudo-dynamic network model, assume that $\widehat{y}_k = K_i \frac{1}{s}(\widehat{i}_k^{ref} - \widehat{I}_{v,k})$, then

$$\begin{aligned} \widehat{y}_k &= y_{k-1} + K_i \frac{T_s}{2}\left(\widehat{i}_k^{ref} - \widehat{I}_{v,k} + i_{k-1}^{ref} - I_{v,k-1}\right), \\ y_{k-1} &= -v_{k-1}^{ref} + V_{k-1} - K_p(i_{k-1}^{ref} - I_{v,k-1}) - j(X_t + X_p) i_{k-1}^{ref}. \end{aligned}$$

Substituting $\widehat{y}_k$ and y_{k-1} into Eq. (15), then

$$\begin{aligned} \mathbf{h(x_k)}: \; & \widehat{v}_k^{ref} - v_{k-1}^{ref} - \widehat{V}_k + V_{k-1} \\ & + K_p\left(\widehat{i}_k^{ref} - \widehat{I}_{v,k} - i_{k-1}^{ref} + I_{v,k-1}\right) \\ & + K_i \frac{T_s}{2}\left(\widehat{i}_k^{ref} - \widehat{I}_{v,k} + i_{k-1}^{ref} - I_{v,k-1}\right) \\ & + j(X_t + X_p)\left(\widehat{i}_k^{ref} - i_{k-1}^{ref}\right). \end{aligned} \tag{16}$$

As all the states at step $(k-1)$ are known, they can be considered as a constant component and are denoted by C. Hence, Eq. (16) can be simplified as

$$\mathbf{h(x_k)}: \ \widehat{v}_k^{ref} - \widehat{V}_k + \left(K_p + K_i\frac{T_s}{2}\right)\left(\widehat{i}_k^{ref} - \widehat{I}_{v,k}\right) + j(X_t + X_p)\widehat{i}_k^{ref} + C. \quad (17)$$

The above equation can be split into d and q components:

$$\begin{aligned}\mathbf{h(x_k)}: \ & \widehat{v}_{d,k}^{ref} - |\widehat{V}_k|cos(\widehat{\theta}_k) + \left(K_p + K_i\frac{T_s}{2}\right)\left(\widehat{i}_{d,k}^{ref}\right. \\ & \left. - |\widehat{I}_{v,k}|cos(\widehat{\delta}_{v,k})\right) - (X_t + X_p)\widehat{i}_{q,k}^{ref} + C_d, \\ & \widehat{v}_{q,k}^{ref} - |\widehat{V}_k|sin(\widehat{\theta}_k) + \left(K_p + K_i\frac{T_s}{2}\right)\left(\widehat{i}_{q,k}^{ref}\right. \\ & \left. - |\widehat{I}_{v,k}|sin(\widehat{\delta}_{v,k})\right) + (X_t + X_p)\widehat{i}_{d,k}^{ref} + C_q. \end{aligned} \quad (18)$$

Thus, the converter bridges' voltage reference v_{ref} can be expressed by Eq. (13) and Eq. (18). So Eq. (11) becomes

$$\mathbf{h(x)} \begin{cases} K_{d2a}M_v\dfrac{V_{dc}}{2} - \sqrt{(v_d^{ref})^2 + (v_q^{ref})^2} \\ (K_{d2a})^2\dfrac{V_{dc}}{2}I_{dc} - |V_v||I_v|\cos(\theta_v - \delta_v). \end{cases} \quad (19)$$

Therefore, Eqs. (10), (19), (13), and (18) constitute the pseudo-dynamic network model for VSC substations. As a result, four more states are added to this pseudo-dynamic model compared to its static model:

$$\mathbf{x} = [|\mathbf{V}|, |\mathbf{I}|, \theta, \delta, |\mathbf{V_f}|, \theta_\mathbf{f}, |\mathbf{I_f}|, \delta_\mathbf{f}, |\mathbf{V_v}|, \theta_\mathbf{v}, \mathbf{V_{dc}}, \mathbf{I_{dc}} \ \mathbf{i_d^{ref}}, \mathbf{i_q^{ref}}, \mathbf{v_d^{ref}}, \mathbf{v_q^{ref}}]^T. \quad (20)$$

The Jacobian matrix needs to be updated w.r.t. Eqs. (13), (18), and (19). Taking the first equation of Eq. (13) as an example, its corresponding Jacobian matrix element w.r.t. voltage magnitude is given by

$$H(x_k): \frac{\partial h(x_k)}{\partial|\widehat{V}_k|} = K_P\frac{T_s}{2}\frac{|\widehat{I}_k|cos(\widehat{\theta}_k - \widehat{\delta}_k)}{|\widehat{V}_{f,k}|}.$$

C. POINT-TO-POINT VSC-HVDC LINK MODEL

Using the VSC substation model constructed above, other VSC models can be developed. The point-to-point VSC-HVDC link is of primary interest here. To model the link, one VSC substation acts as the rectifier and the other one as the inverter, depending on which side controls the active power flow. At each substation a large DC capacitor is installed, and a DC cable connects two substations [29]. The DC circuit of a point-to-point VSC-HVDC link model is shown in Fig. 5 and the basic equations are:

$$\mathbf{h(x)} \begin{cases} C_{dc}\dfrac{dV_{dc1}}{dt} - (I_{dc1} - I_{cc}), \\ C_{dc}\dfrac{dV_{dc2}}{dt} - (I_{dc2} + I_{cc}), \\ L_{dc}\dfrac{dI_{cc}}{dt} - (V_{dc1} - V_{dc2} - R_{dc}I_{cc}). \end{cases} \quad (21)$$

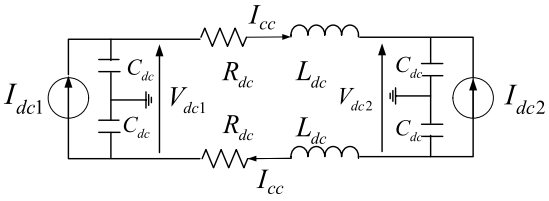

FIGURE 5. DC circuit of a point-to-point VSC-HVDC link model.

The corresponding pseudo-dynamic equations are:

$$\begin{aligned}\mathbf{h(x_k)}: \ & \widehat{V}_{dc1,k} - \frac{T_s}{2C_{dc}}\widehat{I}_{dc1,k} + \frac{T_s}{2C_{dc}}\widehat{I}_{cc,k} - V_{dc1,k-1} \\ & - \frac{T_s}{2C_{dc}}\widehat{I}_{dc1,k-1} + \frac{T_s}{2C_{dc}}\widehat{I}_{cc,k-1}, \\ & \widehat{V}_{dc2,k} - \frac{T_s}{2C_{dc}}\widehat{I}_{dc2,k} - \frac{T_s}{2C_{dc}}\widehat{I}_{cc,k} - V_{dc2,k-1} \\ & - \frac{T_s}{2C_{dc}}\widehat{I}_{dc2,k-1} - \frac{T_s}{2C_{dc}}\widehat{I}_{cc,k-1}, \\ & (1 + \frac{T_sR_{dc}}{2L_{dc}})\widehat{I}_{cc,k} - \frac{T_s}{2L_{dc}}\widehat{V}_{dc1,k} + \frac{T_s}{2L_{dc}}\widehat{V}_{dc2,k} \\ & - (1 - \frac{T_sR_{dc}}{2L_{dc}})I_{cc,k-1} - \frac{T_s}{2L_{dc}}V_{dc1,k-1} \\ & + \frac{T_s}{2L_{dc}}V_{dc2,k-1}. \end{aligned} \quad (22)$$

V. CASE STUDY

This section focuses on studying the performance of the PMU-based SEs accuracy when using the static network model and the proposed pseudo-dynamic network model. Subsection V-A uses real PMU data to compare and validate these two models in the case of a STATCOM. In Subsection V-B, two test systems with a STATCOM installed were built up and simulated in PSAT to generate the synthetic measurements for the accuracy comparison. At last, the *VSC-Based HVDC Link model* provided by MATLAB/*Simulink* was used to generate synthetic measurements for two test scenarios used in the comparisons in Subsection V-C.

A. STATCOM MODELS COMPARISON AND VALIDATION USING REAL PMU DATA

The real PMU data used in this subsection was recorded during a generator trip event. The generator loss resulted in reducing the active power flow on the main transfer paths in a neighboring system, and caused an increase in bus voltages. A STATCOM installed on the transfer paths reacted to the voltage change. The STATCOM bus voltage phasor, as well as its output current phasor, was measured by a PMU with a reporting rate of 30 *samples*/*second*.

Figure 6 shows the STATCOMs V-I curve computed using the PMU data. Blue dots represent pre-fault operation points, which depict a linear V-I characteristic. When the fault occurred, several green dots scatter away from the V-I characteristic. Gradually the system reached another

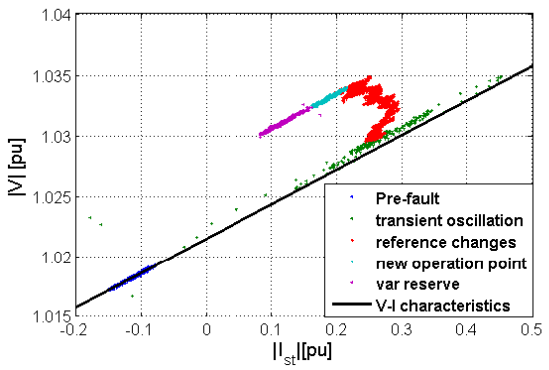

FIGURE 6. The STATCOM PMU measurements and linear V-I characteristic.

stable operation point where the STATCOM current is about 0.25 $p.u$. Note that the STATCOM's output current switched from capacitive to inductive after the disturbance occurred, aiming to decrease the bus voltage. When the system was approaching the next steady state, the system operator changed the voltage reference of the STATCOM in several steps, which can be seen from the saw-tooth variation in red (the voltage reference corresponds to the voltage when the STATCOM current output equals to zero). The system reached a new operation point after the reference changed, which is represented by the light blue dots. As the system turned to a new steady state condition, the system operator switched the STATCOM to the var reserve control mode such that other slower voltage controls in the system can take over the reactive power support.

Figure 6 shows the variation of operating conditions during the whole event and clearly reveals the linear V-I droop relation of a STATCOM in steady-state operation. Using the pre-fault PMU data (0 to 69.33s), this linear V-I characteristic was determined by applying the linear regression function `polyfit` in MATLAB, which is shown by the black line in Fig. 6. The two coefficients of the linear predictor, slope and the intercept, represent the equivalent impedance and voltage reference of the STATCOM, respectively. For the pre-fault steady state, $X_s = 0.0285$ and $V^{ref} = 1.0214$.

Note that during the transients, the operating points scatter and do not exactly follow the V-I characteristic. For a certain $|V|$, the measured $|I_{st}|$ and the read value from the V-I characteristic can deviate up to 0.04 $p.u$. This implies that the static STATCOM model, which is based on the V-I characteristic, would result in deviations during transients.

On the other hand, the pseudo-dynamic model can be a good choice to reflect the STATCOM's control process and its system dynamics. Using the transfer function estimator `tfest` in MATLAB, the transfer function is estimated as $\frac{32.1981}{0.0329s+1}$, with two control parameters $K = 32.1981$ and $T = 0.0329$, which are those in Eqs. (7)-(9).

The gain K theoretically is the reciprocal of the V-I characteristics' slope. For the transient oscillation period, the slope calculated by the linear regression is $X_s = 0.0285$, whose inverse (32.1543) is quite close to the calculated K (32.1981). which verifies that of the transfer function. In addition, the time constant T is in accordance with the statement of STATCOM in [26], which says "typically about 10-50 ms depending on the var generator transport lag".

In order to intuitively compare the STATCOM's static model with its pseudo-dynamic model, PMU data of the voltage magnitude $|V|$ is used as the arbitrary inputs of the static model (see Eq. (5)) and the pseudo-dynamic model (see Eqs. (7)-(9)), respectively. The static model applies the STATCOM's linear V-I characteristic and the pseudo-dynamic model applies its first-order control model whose parameters were obtained above through model identification. These models' outputs are then compared to the $|I_{st}|$ PMU measurement in Fig. 7.

Figure 7 compares results: the pseudo-dynamic model' output $|I_{st}|$ coincides with the PMU data; while the static model's output gradually deviates from the the PMU data. The reason that the deviation is not prominent is because the time constant of the STATCOM is quite close to the PMU sampling rate, thereby its dynamical trajecory can be nearly tracked by the PMU measurement. For a larger and more complex system, this deviation could be amplified further. An analysis of their residuals w.r.t. the PMU data is shown in Table 1.

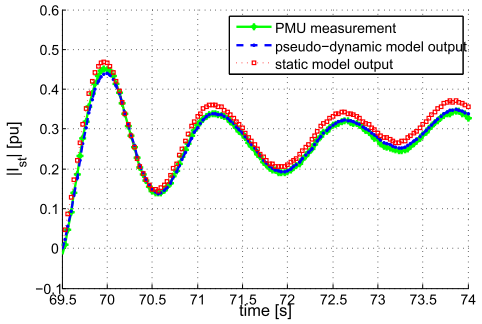

FIGURE 7. PMU data, static model output and pseudo-dynamic model output for the current at the STATCOM.

TABLE 1. STATCOM models accuracy comparison.

SE methods	μ^*	δ^{**}	Max. residual
Pseudo-dynamic	0.0012	0.0056	0.0152
Static	0.0198	0.0085	0.0406

$^*\mu$ denotes the average value of the residuals w.r.t. the PMU data

$^{**}\delta$ denotes the standard deviation of the residuals w.r.t. the PMU data

B. STATCOM MODEL IN TWO TEST SYSTEMS

Next, in order to further study the proposed STATCOM model and PMU-based SE algorithm, a modified WSCC 3-machine 9-bus test system and a modified KTH-Nordic 32 test system are used. Their one-line diagrams can be

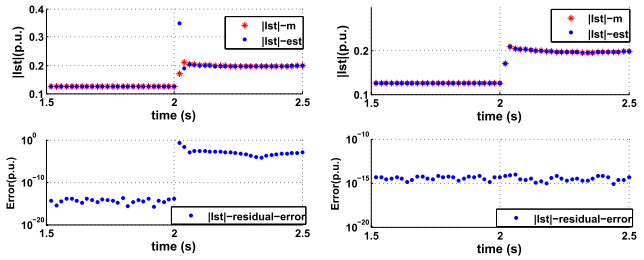

FIGURE 8. Static and Pseudo-dynamic PMU-based SEs of the modified WSCC 3-machine 9-bus test system. (a) $|I_{st}|$ static. (b) $|I_{st}|$ pseudo-dynamic.

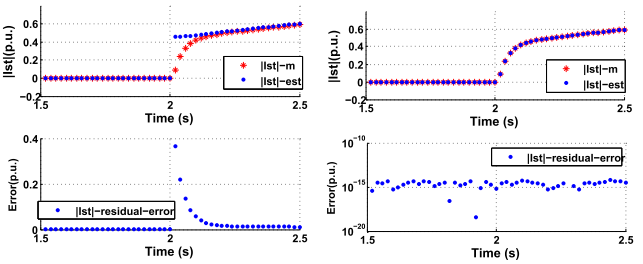

FIGURE 9. Static and Pseudo-dynamic PMU-based SEs of the modified KTH-Nordic 32 test system. (a) $|I_{st}|$ static. (b) $|I_{st}|$ pseudo-dynamic.

found in [16] and [30], respectively. In the modified WSCC 3-machine 9-bus test system, a STATCOM is installed at Bus 8; in the modified KTH-Nordic 32 test system, the same STATCOM is installed at Bus 43. Its two important parameters are $K = 25$, $T = 0.04$. Synthetic measurements for off-line SE computations were obtained by running time-domain simulations in the Power System Analysis Toolbox (PSAT) [31], and 20 *ms* is selected as the step-size to imitate the PMU data rate. For these tests, no measurement noise was added because we aim to focus on the influences of two network models on the SE accuracy. All the weightings of the network equations and measurements are assumed to be 1, and full measurement observability is assumed.

1) TEST ON THE MODIFIED WSCC 3-MACHINE 9-BUS SYSTEM

A 16.67% load increase (both active power and reactive power) at Bus 8 was applied at $t = 2s$. As shown in Fig. 8, for both cases the current magnitude residuals before the perturbation occurred are below $10^{-13} p.u.$; however, after the instance when the perturbation occurred, the static PMU-based SE residuals increase up to 0.1783 $p.u.$ then drop to $10^{-3} p.u.$ while the pseudo-dynamic PMU-based SE successfully stays on the same level during transient dynamics. More estimation accuracy performances are shown in Table 2.

2) TEST ON THE MODIFIED KTH-NORDIC 32 SYSTEM

A 33% load increase (both active power and reactive power) at Bus 43 was applied at $t = 2s$. As shown in Fig. 9, the static SE and pseudo-dynamic SE hold similar SE accuracy of the current magnitude before the perturbation. However, after the perturbation occurs, the current magnitude estimated by the static SE shows a residual up to 0.3666 $p.u.$ On the other hand, the pseudo-dynamic SE gives a maximum residual of $5.0626 \times 10^{-14} p.u.$ Table 2 summaries the results of these tests.

C. VSC-HVDC MODEL

There are many VSC-HVDC simulation models proposed in the literature. However, in order to make the test system accessible by other researchers, the *VSC-Based HVDC Transmission Link model* provided by MATLAB R2013B/*SimPowerSystems* is used to generate synthetic measurements to validate the proposed VSC-HVDC model and PMU-based SE algorithm. A detailed description of the model and control strategy can be found in [32]. All the control parameters preset in the *Simulink* model are kept the same in the pseudo-dynamic SE model. The measurements generated by simulating the *VSC-Based HVDC Link model* are then re-sampled with 20 *ms* rate to imitate the PMU data rate.

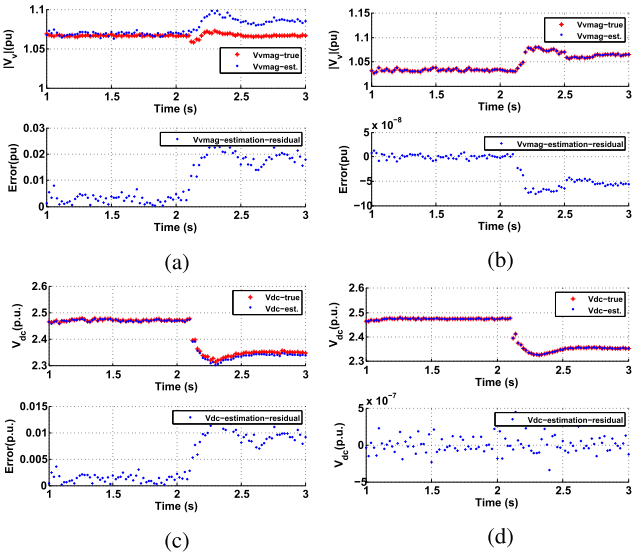

FIGURE 10. Static and Pseudo-dynamic PMU-based SEs of the VSC-HVDC link test system's first test scenario. (a) $|V_V|$ static. (b) $|V_V|$ pseudo-dynamic. (c) V_{dc} static. (d) V_{dc} pseudo-dynamic.

1) FIRST TEST SCENARIO

The inverter's DC voltage reference dropped from 1 $p.u.$ to 0.95 $p.u.$ at $t = 2.1s$. As shown in Fig. 10, the pseudo-dynamic SE performs more accurately by a factor of 1/1000 than the static SE not only during transients, but also during steady state. For instance, the voltage magnitudes on the rectifier side estimated by the static SE shows a maximum residual up to 0.0279 $p.u.$ while the pseudo-dynamic SE gives a maximum residual of $7.6517 \times 10^{-8} p.u.$

TABLE 2. SE accuracy performance on test systems.

		Before perturbation (μ, σ)		After perturbation (μ, σ)		Max. residual	
		static	pseudo-dynamic	static	pseudo-dynamic	static	pseudo-dynamic
STATCOM test1	$Res.\|V_8\|$	(1.57e-16, 1.02e-16)	(1.57e-16, 1.02e-16)	(3.85e-16, 1.27e-15)	(7.25e-16, 1.76e-15)	7.11e-15	8.22e-15
	$Res.\|I_{st}\|$	(-3.84e-15, 9.58e-15)	(-3.72e-15, 2.01e-15)	(8.03e-04, 0.0127)	(-3.57e-15, 2.16e-14)	0.1783	1.05e-13
STATCOM test2	$Res.\|V_{43}\|$	(-8.71e-17, 7.13e-17)	(-8.71e-17, 7.13e-17)	(-2.94e-17, 2.12e-16)	(-2.39e-17, 1.95e-16)	2.44e-15	2.22e-15
	$Res.\|I_{st}\|$	(-2.06e-16, 6.37e-15)	(2.11e-15, 1.83e-15)	(0.0048, 0.0332)	(1.57e-15, 7.16e-15)	0.3666	5.06e-14
VSC-HVDC test1	$Res.\|V_v\|$	(0.0023, 0.0024)	(5.45e-10, 4.74e-09)	(0.0187, 0.0039)	(-5.39e-08, 1.78e-08)	0.0279	7.65e-08
	$Res.\|I_v\|$	(-0.0091, 0.0035)	(-1.59e-08, 4.37e-07)	(-0.0135, 0.0042)	(5.60e-08, 2.36e-06)	0.0214	1.04e-05
	$Res.V_{dc}$	(-0.0012, 0.0010)	(-6.60e-10, 1.09e-07)	(-0.0094, 0.0021)	(1.05e-08, 1.25e-07)	0.0141	4.44e-07
	$Res.I_{dc}$	(0.0108, 0.0041)	(-3.46e-11, 2.00e-09)	(0.0148, 0.0045)	(2.00e-08, 7.62e-09)	0.0237	2.81e-08
VSC-HVDC test2	Res. $\|V_v\|$	(0.0023, 0.0024)	(5.45e-10, 4.74e-09)	(-0.0131, 0.0423)	(-1.62e-08, 3.77e-08)	0.0207	1.87e-07
	Res. $\|I_v\|$	(-0.0091, 0.0035)	(-1.59e-08, 4.37e-07)	(-0.0059, 0.0174)	(1.18e-06, 1.84e-05)	0.0824	8.15e-05
	Res.V_{dc}	(-0.0012, 0.0010)	(-6.60e-10, 1.09e-07)	(0.0026, 0.0119)	(9.57e-07, 9.75e-07)	0.0400	3.44e-06
	Res. I_{dc}	(0.0108, 0.0041)	(-3.46e-11, 2.00e-09)	(0.0068, 0.0307)	(1.01e-08, 5.23e-08)	0.1418	2.95e-07

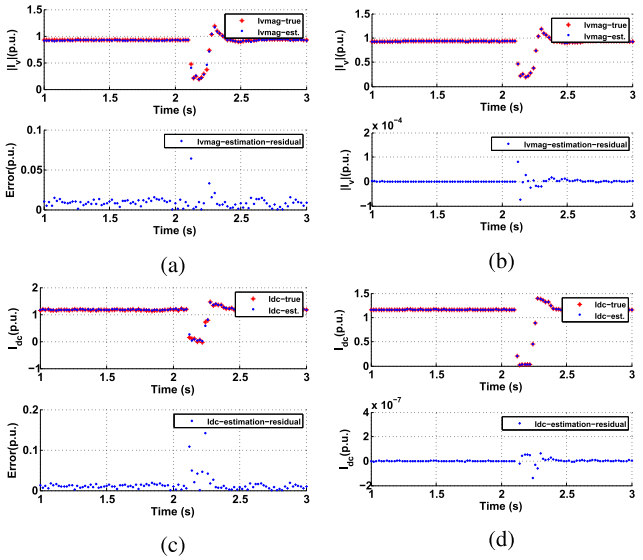

FIGURE 11. Static and Pseudo-dynamic PMU-based SEs of the VSC-HVDC link test system's second test scenario. (a) $|I_V|$ static. (b) $|I_V|$ pseudo-dynamic. (c) I_{dc} static. (d) I_{dc} pseudo-dynamic.

2) SECOND TEST SCENARIO

A three-phase line breaker on the inverter side was opened from $t = 2.1s$ for $0.12s$. For this larger perturbation, as shown in Fig. 11, the pseudo-dynamic SE performs more accurately by a factor of $1/1000$ than the static SE. For instance, the DC current estimated by the static SE shows a maximum residual up to $0.1418\,p.u.$ while the pseudo-dynamic SE gives a maximum residual of $2.9504 \times 10^{-7} p.u.$ Table 2 summaries the results of these tests.

As it might be noted that in Figs. 8 and 9 both static and pseudo dynamic models maintain almost the same level of accuracy during normal operation (order of 10^{-15}) while in Figs. 10 and 11 improvement during normal operation is seen for the pseudo dynamic model. The reason is the pseudo-dynamic model is capable to include internal states that are calculated in real-time, such as the voltage reference used in Section IV. In contrast, static models do not possess such flexibility.

TABLE 3. Computation performance comparison.

PMU-based SE method	Aver. comp. time per snapshot	Aver. no. of iter. per snapshot	Largest no. of iteration
P-dynamic	4.754 ms	5.465	10
Static	3.115 ms	5.525	11

VI. SE COMPUTATION PERFORMANCE

One advantage of the proposed pseudo-dynamic PMU-based SE is that it does not significantly increase the computation complexity and burden when compared to the static SE. By comparing the number of iterations and computation time of the static and the pseudo-dynamic PMU-based SEs, as shown in Table 3, it can be seen that the pseudo-dynamic SE performs similarly to the static SE in terms of computation speed. These SE computations were carried out on the VSC-HVDC test scenario I using an ordinary PC with an Intel(R) Core(TM) i7-2640M CPU @2.80GHz and a 8.00 GB RAM, and using MATLAB R2013B.

VII. CONCLUSION

This article presents a PMU-based state estimator using a pseudo-dynamic network model. This method significantly improves the SE accuracy during transients as compared to the static PMU-based SE. In contrast to most dynamic SE algorithms, it implements an iterative algorithm to update the estimated states instead of solving differential and algebraic equations (DAEs), which significantly saves computational resources. Additionally, the pseudo-dynamic network model can be easily constructed from the original static model and represent devices with time-varying control references.

The second major contribution of this article is the pseudo-dynamic network models for STATCOMs and VSC-HVDCs. These two models also provide valuable and practical insight on how to develop pseudo-dynamic network models for components and controllers in power systems.

The case studies provide sufficient evidence that the pseudo-dynamic SE algorithm is capable of performing much more accurate estimation during transient dynamics without significantly increasing the computation resources as compared to the static SEs. The STATCOM using real PMU data shows that the proposed modeling approach and PMU-based algorithm is applicable when real PMU data from actual power systems is available.

Future work will focus on testing the proposed approach under noisy measurements w.r.t. the computational burden of the SE.

REFERENCES

[1] S. G. Ghiocel *et al.*, "Phasor-measurement-based state estimation for synchrophasor data quality improvement and power transfer interface monitoring," *IEEE Trans. Power Syst.*, vol. 29, no. 2, pp. 881–888, Mar. 2014.

[2] E. R. Fernandes *et al.*, "Application of a phasor-only state estimator to a large power system using real PMU data," *IEEE Trans. Power Syst.*, vol. 32, no. 1, pp. 411–420, Jan. 2017.

[3] L. Vanfretti, J. H. Chow, S. Sarawgi, and B. Fardanesh, "A phasor-data-based state estimator incorporating phase bias correction," *IEEE Trans. Power Syst.*, vol. 26, no. 1, pp. 111–119, Feb. 2011.

[4] A. G. Phadke, and J. S. Thorp, *Synchronized Phasor Measurements and Their Applications*. New York, NY, USA: Springer-Verlag, 2008.

[5] N. Zhou and Z. Huang. PNNL, WA, USA. (Mar. 2014). *Capturing Dynamics in the Power Grid: Formulation of Dynamic State Estimation Through Data Assimilation*. [Online]. Available: http://www.pnnl.gov/main/publications/external/technical_reports/PNNL-23213.pdf

[6] F. C. Schweppe and R. D. Masiello, "A tracking static state estimator," *IEEE Trans. Power App. Syst.*, vol. PAS-90, no. 3, pp. 1025–1033, May 1971.

[7] A. S. Debs and R. E. Larson, "A dynamic estimator for tracking the state of a power system," *IEEE Trans. Power App. Syst.*, vol. PAS-89, no. 7, pp. 1670–1678, Sep. 1970.

[8] M. B. D. C. Filho and J. C. S. de Souza, "Forecasting-aided state estimation—Part I: Panorama," *IEEE Trans. Power Syst.*, vol. 24, no. 3, pp. 1667–1677, Nov. 2009.

[9] H. R. Sirisena and E. P. M. Brown, "Composite hydroelectric energy system state estimation," *IFAC Proc. Volumes*, vol. 20, no. 6, pp. 399–404, 1987.

[10] B. Xu, and A. Abur, "State estimation of systems with embedded FACTS devices," in *Proc. IEEE PowerTech Conf.*, Jun. 2003, p. 5.

[11] C. Rakpenthai, S. Premrudeepreechacharn, and S. Uatrongjit, "Power system with multi-type FACTS devices state estimation based on predictor–corrector interior point algorithm," *Int. J. Elect. Power Energy Syst.*, vol. 31, no. 4, pp. 160–166, May 2009.

[12] A. Zamora-Cárdenas, C. R. Fuerte-Esquivel, "State estimation of power systems containing FACTS controllers," *Electr. Power Energy Syst.*, vol. 81, no. 4, pp. 995–1002, Apr. 2011.

[13] P. I. Bartolomey, S. A. Eroshenko, E. M. Lebedev, and A. A. Suvorov, "New information technologies for state estimation of power systems with FACTS," in *Proc. IEEE PES (ISGT Europe)*, Oct. 2012, pp. 1–8.

[14] E. A. Zamora-Cárdenas, B. A. Alcaide-Moreno, and C. R. Fuerte-Esquivel, "State estimation of flexible AC transmission systems considering synchronized phasor measurements," *Electr. Power Syst. Res.*, vol. 106, pp. 120–133, Jan. 2014.

[15] V. I. Presada, C. V. Cristea, M. Eremia, and L. Toma, "State estimation in power systems with FACTS devices and PMU measurements," in *Proc. UPEC*, Sep. 2014, pp. 1–5.

[16] W. Li and L. Vanfretti, "A PMU-based state estimator for networks containing FACTS devices," in *Proc. IEEE PES PowerTech*, Jun./Jul. 2015, pp. 1–6.

[17] H. R. Sirisena and E. P. M. Brown, "Inclusion of HVDC links in AC power-system state estimation," *IEE Proc. C-Generat., Transmiss. Distrib.*, vol. 128, no. 3, pp. 147–154, May 1981.

[18] Q. Ding, B. Zhang, and T. S. Chung, "State estimation for power systems embedded with FACTS devices and MTDC systems by a sequential solution approach," *Electr. Power Syst. Res.*, vol. 55, no. 3, pp. 147–156, Sep. 2000.

[19] W. Li and L. Vanfretti, "A PMU-based state estimator considering classic HVDC links under different control modes," *Sustain. Energy, Grids Netw.*, vol. 2, pp. 69–82, Jun. 2015.

[20] A. de la Villa Jaén, E. Acha, and A. G. Expósito, "Voltage source converter modeling for power system state estimation: STATCOM and VSC-HVDC," *IEEE Trans. Power Syst.*, vol. 23, no. 4, pp. 1552–1559, Nov. 2008.

[21] J. Cao, W. Du, and H. F. Wang, "The incorporation of generalized VSC MTDC model in AC/DC power system state estimation," in *Proc. SUPERGEN*, Sep. 2012, pp. 1–6.

[22] E. A. Zamora-Cárdenas, C. R. Fuerte-Esquivel, A. Pizano-Martínez, and H. J. Estrada-García, "Hybrid state estimator considering SCADA and synchronized phasor measurements in VSC-HVDC transmission links," *Electr. Power Syst. Res.*, vol. 133, pp. 42–50, Apr. 2016.

[23] W. Li and L. Vanfretti, "A PMU-based state estimator for networks containing VSC-HVDC links," in *Proc. IEEE PES General Meeting*, Jul. 2015, pp. 1–5.

[24] P. Yang, Z. Tan, A. Wiesel, and A. Nehorai, "Placement of PMUs considering measurement phase-angle mismatch," *IEEE Trans. Power Del.*, vol. 30, no. 2, pp. 914–922, Apr. 2015.

[25] M. S. Almas, L. Vanfretti, R. S. Singh, and G. M. Jonsdottir, "Vulnerability of synchrophasor-based WAMPAC applications' to time synchronization spoofing," *IEEE Trans. Smart Grid*, to be published.

[26] N. G. Hingorani and L. Gyugyi, "Static shunt compensators: SVC and STATCOM," in *Understanding FACTS: Concepts and Technology of Flexible AC Transmission Systems*. New York, NY, USA: IEEE Press, 2000, ch. 5.

[27] K. K. C. Yu and N. R. Watson, "An approximate method for transient state estimation," *IEEE Trans. Power Del.*, vol. 22, no. 3, pp. 1680–1687, Jul. 2007.

[28] L. Harnefors and H.-P. Nee, "Model-based current control of AC machines using the internal model control method," *IEEE Trans. Ind. Appl.*, vol. 34, no. 1, pp. 133–141, Jan./Feb. 1998.

[29] S. Cole, J. Beerten, and R. Belmans, "Generalized dynamic VSC MTDC model for power system stability studies," *IEEE Trans. Power Syst.*, vol. 25, no. 3, pp. 1655–1662, Aug. 2010.

[30] Y. Chompoobutrgool, W. Li, and L. Vanfretti, "Development and implementation of a nordic grid model for power system small-signal and transient stability studies in a free and open source software," in *Proc. IEEE PES Gen. Meeting*, Jul. 2012, pp. 1–8.

[31] F. Milano, "An open source power system analysis toolbox," *IEEE Trans. Power Syst.*, vol. 20, no. 3, pp. 1199–1206, Aug. 2005.

[32] R2015b. MathWorks, Inc. Natick, MA, USA. *VSC-Based HVDC Link*. [Online]. Available: http://se.mathworks.com/help/physmod/sps/powersys/ug/vsc-based-hvdc-link.html

WEI LI received the B.S. degree in automation from Beijing Jiaotong University, in 2010 and the M.S. degree in electronics design from Mid Sweden University, in 2011. She is currently working toward the Ph.D. degree at the Electric Power and Energy Systems Division, KTH. The main theme of her current research is the real-time wide-area state estimation of hybrid ac and dc grids.

LUIGI VANFRETTI (SM'14) received the M.Sc. and Ph.D. degrees in electric power engineering from the Rensselaer Polytechnic Institute, Troy, NY, USA, in 2007 and 2009, respectively. He was with the KTH Royal Institute of Technology, Stockholm, Sweden, as an Assistant from 2010 to 2013, and as an Associate Professor (Tenured) and a Docent from 2013to 2017, where he led the SmarTS Lab and Research Group. He was with the Statnett SF, the Norwegian electric power transmission system operator, as a Consultant from 2011 to 2012, and as a Special Advisor in research and development, from 2013 to 2016. He joined the Rensselaer Polytechnic Institute in 2017, where he is currently a tenured Associate Professor. His research interests are in the area of synchrophasor technology applications; and cyber-physical power system modeling, simulation, stability, and control.

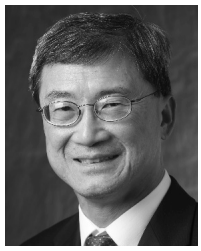

JOE H. CHOW (S'72–M'78–SM'84–F'92–LF'17) received the B.S. degree from the University of Minnesota and the M.S. and Ph.D. degrees from the University of Illinois, Urbana–Champaign. He was with General Electric Power System Business, Schenectady. He joined the Rensselaer Polytechnic Institute in 1987, where he is currently a Professor of Electrical, Computer, and Systems Engineering. He is also the RPI Campus Director of the National Science Foundation/Department of Energy and Current European Research Council. His research interests include multivariable control, power system dynamics and control, control of renewable resources, and synchronized phasor data. He was a recipient of the IEEE PES Charles Concordia Award in 2014. In 2017, he was elected to the National Academy of Engineering and named Institute Professor of Engineering by the Rensselaer Polytechnic Institute.